JOURNAL OF GEOPHYSICAL RESEARCH, VOL. 99, NO. A7, PAGES 13,455–13,464, JULY 1, 1994

Alfvén resonance excitation and fast wave propagation in magnetospheric waveguides

Graham J. Rickard and Andrew N. Wright

Department of Mathematical and Computational Sciences, University of St Andrews, St Andrews Fife, Scotland

Abstract. Magnetic pulsations are a robust feature of the Earth's magnetosphere. It has been suggested recently that the magnetosphere is sometimes better modeled as a waveguide rather than a cavity. This paper presents numerical simulations of linear magnetohydrodynamic (MHD) waves in an inhomogeneous, low-β waveguide. Several features predicted by recent theoretical studies are confirmed in our simulations, notably that Alfvén resonances are driven at frequencies corresponding to the natural frequency of the fast waveguide modes with $V_g \approx 0$ ($k_y \approx 0$).

1. Introduction

A characteristic signature of the Earth's magnetosphere is that provided by so-called magnetic pulsations. This paper concentrates upon the type of pulsations commonly referred to as toroidal or azimuthal Alfvén pulsations. Over a wide range of magnetospheric conditions it is observed that the natural frequencies associated with these pulsations remain largely unaltered. This result is surprising, given the rich variety of possible wave structures that a three-dimensional magnetosphere can produce. The challenge is to provide an explanantion for these results.

The resonant coupling of fast and Alfvén waves in a magnetospheric context dates back to the studies of *Southwood* [1974] and *Chen and Hasegawa* [1974]. More recently, the "cavity mode model" of *Kivelson and Southwood* [1985] has enjoyed much success in explaining observations and features of numerical solutions [*Allan et al.*, 1986, *Inhester*, 1987, *Lee and Lysak*, 1989].

Plasmaspheric pulsations may be considered as existing in an approximately axisymmetric cavity. Azimuthal and field aligned wave numbers together with radial boundary conditions determine a discrete set of fast mode eigenfrequencies. These fast cavity modes may drive a discrete set of Alfvén resonances (pulsations).

Pulsations in the middle and outer magnetosphere ($L \gtrsim 5$) cannot be thought of as existing in a cavity; this region of the magnetosphere is not axisymmetric and has an open-ended magnetotail. Recent studies by *Samson et al.* [1992] and *Walker et al.* [1992] sugggest that we treat this part of the magnetosphere as an inhomogeneous *waveguide* rather than a cavity.

The idea of a waveguide in magnetospheric and solar plasmas is not new. The geomagnetic tail has been described as a waveguide for over a quarter of a century [*McClay and Radoski*, 1967, *Hopcraft and Smith*, 1986, *Edwin et al.*, 1986]. The propagation and dispersive properties of the fast wave in an MHD waveguide have also been developed for solar coronal applications using identical equations to those previously investigated in the context of ducted seismic and oceanographic waves [see *Roberts et al* [1984], and references therein]. However, it is only recently that the notion of a waveguide has been applied to the dawn and dusk flanks of the magnetosphere [*Walker et al.*, 1992]. The flanks produce a waveguide in which the equilibrium field is directed across the the guide, in contrast to the tail waveguide which has the field along the guide. The characteristic dispersion in these two models is quite different [*Edwin et al.*, 1986, *Wright*, 1994].

One important difference between a waveguide and a cavity is that the absence of boundaries along the guide allows the wave number in that direction to adopt a continuous range of values. Thus the natural frequencies of the fast waveguide modes do not have a discrete spectrum as in the cavity model, and it is not obvious why Alfvén resonances (pulsations) should be excited at particular frequencies. *Harrold and Samson* [1992] circumvented this problem by considering solutions with a single value of k_y, thus producing a discrete set of fast eigenfrequencies. Both *Walker et al* [1992] and *Wright* [1994] have proposed mechanisms that should excite pulsations at the $k_y = 0$ fast eigenfrequencies. In this paper we investigate the mechanisms suggested by *Wright* [1994].

The waveguide theory developed to date provides qualitative rather than quantitative results concerning the magnetosphere. In an attempt to redress the balance this paper presents numerical simulations of MHD wave propagation in a waveguide. The simulations form a half-way house towards a "complete" description in that the qualitative theory can be readily tested but that true magnetospheric parameters still remain out of reach. However, we believe the behavior found in the present waveguide simulations to be generic of inhomogeneous waveguides and should be a useful guide to predicting and interpreting features of more realistic waveguides.

Paper number 94JA00674.
0148-0227/94/94JA-00674$05.00

Numerical simulations have of course been applied to the cavity model in the past [*Allan et al.*, 1986, *Inhester*, 1987, *Lee and Lysak*, 1989]. To our knowledge, this is the first time that an open-ended waveguide (as opposed to a cavity) has been modeled. The open waveguide is not conceptually difficult to simulate, although it can consume large amounts of computer time.

The layout of the paper is as follows. In section 2 we present the basic equations defining the waveguide model. A brief review of the theoretical background is also given, along with some predictions relevant to our simulations. The numerical method is outlined is outlined in section 3, followed by the results in section 4. We close with some conclusions and a discussion concerning our results.

2. Theory

Our magnetospheric waveguide is based upon the traditional hydromagnetic box model of *Kivelson and Southwood* [1986], which has uniform magnetic field $\mathbf{B} = B\hat{\mathbf{z}}$, $\hat{\mathbf{x}}$ represents the radial direction, and $\hat{\mathbf{y}}$ is a coordinate around the Earth. In the waveguide model we allow the box to have an infinite length in y. The (x, y) coordinates are then better interpreted as distance across the waveguide and distance around the flanks and on into the magnetotail, respectively (see Figure 1). The density is solely a function of x. The boundaries at $x = 0$ and $x = x_m$ are taken to be perfectly reflecting ($\xi_x = 0$), as are the ionospheric boundaries represented by planes at constant z on which the displacement $\boldsymbol{\xi}$ vanishes.

For simplicity we assume the plasma to have a low β, so our model approximates magnetospheric plasma better than the magnetosheath plasma. Neglecting resistivity the governing equations for the linear plasma displacement ($\boldsymbol{\xi}$) and the compressional magnetic field (b_z) perturbations are

$$\frac{1}{V^2}\frac{\partial^2 \xi_x}{\partial t^2} - \frac{\partial^2 \xi_x}{\partial z^2} = -\frac{1}{B}\frac{\partial b_z}{\partial x} \tag{1}$$

$$\frac{1}{V^2}\frac{\partial^2 \xi_y}{\partial t^2} - \frac{\partial^2 \xi_y}{\partial z^2} = -\frac{1}{B}\frac{\partial b_z}{\partial y} \tag{2}$$

$$b_z = -B\left(\frac{\partial \xi_x}{\partial x} + \frac{\partial \xi_y}{\partial y}\right) \tag{3}$$

where $V = B/\sqrt{\mu_0 \rho}$ is the local Alfvén speed and ρ the plasma density.

Any disturbance in the waveguide may be written as a sum over the normal modes of the guide. For each mode we may prescribe wave numbers in the $\mathbf{y}$ and $\hat{\mathbf{z}}$ directions. Note that ionospheric boundary conditions requiring $\boldsymbol{\xi} = 0$ quantizes the wave number k_z. Thus a general disturbance would involve a Fourier *sum* over all permissable k_z. There are no boundary conditions in y to quantize k_y, and accordingly k_y may take a continuous range of values. A general disturbance in y will involve a Fourier *integral* over k_y (which may be thought of as the limit of a Fourier *sum*).

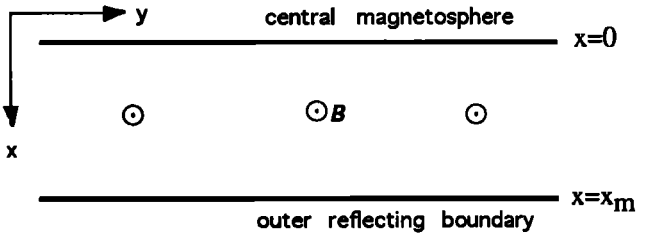

Figure 1. Geometry of the magnetospheric waveguide.

Once k_y and k_z have been chosen we need to solve for the variation in x and the frequency ω of the mode. Seeking normal modes of the form $b_z(x) \exp i[\omega t \pm k_y y \pm k_z z]$, the governing equations (1)-(3) yield the following familiar equation for b_z:

$$\frac{\mathrm{d}^2 b_z}{\mathrm{d}x^2} - \frac{\omega^2 \mathrm{d}V^{-2}/\mathrm{d}x}{\omega^2/V^2 - k_z^2}\frac{\mathrm{d}b_z}{\mathrm{d}x} + \left(\frac{\omega^2}{V^2} - k_y^2 - k_z^2\right) b_z = 0. \tag{4}$$

This equation has a singularity at x_r, where

$$\omega^2 = {k_z}^2 V^2(x_r) \tag{5}$$

and corresponds to the position where the local Alfvén frequency matches the frequency of the waveguide mode.

In the lowest-order WKB analysis we may neglect the second term in (4) and solve the following reduced wave equation in the propagating region [*Inhester*, 1987, *Wright*, 1994]:

$$\frac{\mathrm{d}^2 b_z}{\mathrm{d}x^2} + \left(\frac{\omega^2}{V^2} - k_y^2 - k_z^2\right) b_z = 0. \tag{6}$$

We see that the effective local wave number in x is given by

$$k_x^2(x, \omega) = \frac{\omega^2}{V^2(x)} - k_y^2 - k_z^2 \tag{7}$$

and note that k_x is now an explicit function of x through the nonuniformity of the Alfvén speed, $V(x)$. Evidently, k_x^2 changes sign about the point x_t, where

$$\omega^2 = V^2(x_t)(k_y^2 + k_z^2). \tag{8}$$

The position x_t is referred to as the turning point. The value of b_z changes from being oscillatory to evanescent in x on crossing x_t. The Bohr-Sommerfeld (or phase integral) condition which the wave must satisfy is

$$\int_{x_t}^{x_m} k_x(x)\mathrm{d}x = (n + \alpha)\pi; \qquad n = 1, 2... \tag{9}$$

The phase factor α is determined by the boundary conditions in x. For example, if the mode is reflected off both boundaries at $x = 0, x_m$, then $\alpha = 0$, whereas if the mode has a turning point then $\alpha = -1/4$. The value of α is actually a weak function of k_y: changing k_y for a given mode may actually introduce or remove a turning point from the solution. However, unless x_t is close to $x = 0$ ($x_t k_x(x_t, \omega) \lesssim O(1)$), α varies very slowly with k_y and may be taken as a constant [*Walker et al.*, 1992, *Wright*, 1994].

For the model waveguide used in the present study (see section 4 for a definition) we have calculated $\omega_n(k_y)$ for the first two modes in x that have a fundamental field-aligned dependence by solving (9). The solutions are shown in Figure 2. The $n = 1$ mode (the fundamental mode in x) always has a turning point, even when $k_y = 0$. The $n = 2$ mode (second harmonic structure in x) has a turning point appear in its solution around $k_y x_m \approx 2$. On the interval $1 < k_y x_m < 3$ the factor α changes essentially from 0 to $-1/4$ for $n = 2$. Rather than calculate the complicated function $\alpha(k_y)$, we simply interpolated the curve over this interval for the second harmonic.

The phase velocity of any mode is simply ω/k_y and may be estimated directly from the dispersion diagram (Figure 2). The group velocity along $\hat{\mathbf{y}}$ of a mode is given by $\partial\omega/\partial k_y$ and so is the gradient of the dispersion diagram. A WKB estimate of the group velocity may be derived. Following *Walker et al.* [1992] and *Wright* [1994], we substitute (7) into (9) and differentiating with respect to k_y, assuming α to be a constant, we find the group velocity in $\hat{\mathbf{y}}$

$$V_g = \frac{\partial\omega}{\partial k_y} = \frac{k_y}{\omega}\langle V^{-2}\rangle^{-1}, \tag{10}$$

where

$$\langle V^{-2}\rangle = \int_{x_t}^{x_m} V^{-2}k_x^{-1}\mathrm{d}x \Big/ \int_{x_t}^{x_m} k_x^{-1}\mathrm{d}x. \tag{11}$$

The resultant group velocity curves are shown in Figure 3. (Note that we have again interpolated the $n = 2$ curve over $1 < k_y x_m < 3$ to allow for the fact that α is a function of k_y.) For very large k_y we see that all the group velocities asymptote to the horizontal dashed line, which represents the Alfvén speed at $x = x_m$ (see *Wright* [1994] for a discussion of the form of the group velocities and a physical interpretation). It is evident from the group velocity diagram that different k_y components of the wave will propagate information along the waveguide at different speeds, and result in dispersive behavior of the fast mode.

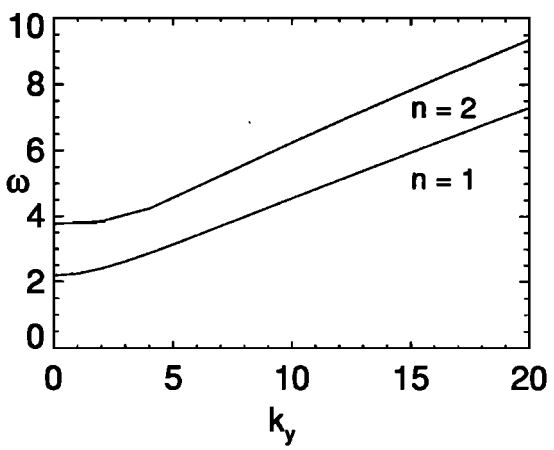

Figure 2. The fast mode dispersion diagram for the first two eigenmodes $n = 1$ and $n = 2$ in the waveguide ($k_z = \pi$).

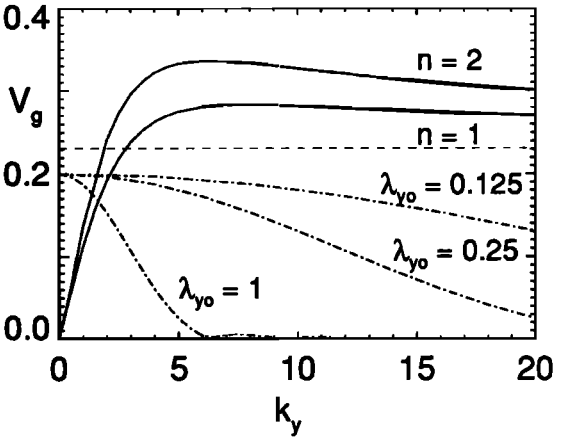

Figure 3. Group velocity V_g against k_y for the dispersion diagram in Figure 2. The horizontal dashed line denotes the asymptotic group velocity of 0.231 for large k_y. The dashed-dotted curves represent the amplitude of the Fourier k_y spectrum of the initial disturbance in y plotted in arbitrary units for different λ_{yo} values (see section 4).

Wright [1994] has argued that a general source of fast mode waves in the waveguide may subsequently excite Alfvén resonances at the natural frequencies of the $k_y \approx 0$ fast waveguide modes. Moreover, these resonances should grow close to the initial fast mode source. These predictions are based upon the fact that for a resonance to grow, the resonant field line must be excited for at least a few cycles with a temporally coherent driver. The resonant Alfvén wave will manifest itself as ξ_y, and from (2) it is apparent that the magnetic pressure gradient in y ($\propto \partial b_z/\partial y$) acts as the driver.

It is also suggested by *Wright* [1994] that natural waveguide dispersion will select modes with $k_y \approx 0$ as the most suitable drivers. The two main reasons being that (1) the natural fast frequency is approximately independent of k_y for small k_y (so the driver has a coherent time dependence), and (2) the $k_y \approx 0$ modes do not propagate along the waveguide, so they may drive a particular field line for several cycles and thereby allow a resonance to develop.

The numerical experiments in the succeeding sections place a disturbance in the waveguide and study the subsequent wave propagation and coupling. We do not address the origin of the initial perturbation. (For example, pressure pulses from the solar wind could hit the magnetopause and propagate a localized fast mode into the magnetospheric waveguide.)

3. Numerical Model

Data shows that the most readily observed pulsations are fundamental along **B**. Accordingly, we shall restrict our attention to a single Fourier mode in z, so that all dependent variables are then functions of x, y, and time t only. Perfectly reflecting conditions are used at each end in x, representing, perhaps, the magnetopause

and plasmapause boundaries. Symmetry conditions at $y = 0$ along the Sun-Earth line are used, while, in keeping with our waveguide model, the other y boundary is taken to be open.

We normalize magnetic field by B, density by $\rho(x)$ at $x = 0$ the plasmapause, and length by the width of the waveguide x_m, say. The characteristic speed is taken to be the Alfvén speed at $x = 0$ ($V(x = 0)$), giving a characteristic time in terms of the Alfvén transit time across the domain, $x_m/V(x = 0)$. In this geometry the governing dimensionless equations reduce to

$$\frac{\partial \mathbf{U}}{\partial t} = \mathbf{F}, \tag{12}$$

where

$$\mathbf{U} = \begin{pmatrix} u_x \\ u_y \\ b_x \\ b_y \\ b_z \end{pmatrix}, \qquad \mathbf{F} = \begin{pmatrix} -(k_z b_x + b_z, x)/\rho \\ -(k_z b_y + b_z, y)/\rho \\ k_z u_x \\ k_z u_y \\ -(u_x, x + u_y, y) \end{pmatrix},$$

where $k_z = 2\pi/\lambda_z$. Here, in the usual notation, b_z, x means partial differentiation of b_z with respect to x. It is clear that we have now expressed the governing set as five first-order partial differential equations (pdes) by introducing $u_x = \xi_x, t$ and $u_y = \xi_y, t$ rather than the three original second-order pdes.

This system is integrated forward in time using the leapfrog-trapezoidal algorithm [*Zalesak*, 1979]. Assuming we know $\mathbf{U}$ at times t and $t - \Delta t$, where Δt is the time step, then

$$\mathbf{U}^\dagger = \mathbf{U}^{t-\Delta t} + 2\Delta t \mathbf{F}^t, \tag{13}$$

$$\mathbf{F}^* = \frac{1}{2}(\mathbf{F}^t + \mathbf{F}^\dagger), \tag{14}$$

$$\mathbf{U}^{t+\Delta t} = \mathbf{U}^t + \Delta t \mathbf{F}^*. \tag{15}$$

The operations in (14) and (15) are used to damp the computational mode inherent in the leapfrog step equation (13); (14) and (15) represent the "trapezoidal" part of the algorithm. The spatial operators in $\mathbf{F}$ are resolved using centered finite differences. Putting these together results in an algorithm that is second-order accurate in both space and time.

The advantage of this algorithm is its simplicity, and boundary conditions are easily incorporated. Its main weaknesses lie in the three-level nature of the scheme. At any instant we need to know $\mathbf{U}$ at two time levels. This means increased storage, as well as the complication of requiring a different time stepping algorithm to start. At present we use a series of small explicit steps with typically a time step of $\Delta t/10$ to find our first new level. Thereafter, the leapfrog-trapezoidal scheme is used. This procedure seems to give accurate results and does not appear to result in any numerical instabilities.

Since we are dealing with a linear system, the fastest propagation speed is known *a priori*. We simply set our fixed time step to be a fraction of the shortest grid transit time. Diagnostic checks on the energy and on the magnetic field divergence reveal that these are conserved to at least six decimal places relative to our of order one normalized system of units. The code solutions also compare favorably with other independent calculations (*I.R. Mann and A.N. Wright* personal communication, 1994) and converge correctly when using reduced time steps and mesh spacings.

We use different (constant) grids spacings in x and y. One of the shortest spatial structures will ultimately develop as a result of phase mixing in the x direction, hence the use of a finer grid in x. As we shall see we impose an initial perturbation that has a given wavelength in y. Our choice for the grid spacing in y is such as to resolve that initial wavelength with the same number of points.

A final issue is the total length of grid to use in the y direction since we are interested in modelling an open waveguide. There are methods for absorbing outgoing waves in an MHD system; however, these are complex to implement and produce some reflection. Since our linear system is so readily updated, we chose the simplest method, namely using a long enough box such that wave reflection would not be a problem. In general, we start with a spatially localized perturbation, and allow the system to evolve for five or six wave characteristic wave periods associated with the resonant field lines. This then sets a total time, which then relates to a total distance given the fast wave speeds in y. This defines the maximum waveguide length. However, as the system evolves, the domain is only completely filled at the very end of the run. This wastes a lot of computing time updating the far end of the waveguide before information has arrived. We therefore start on a shorter grid and run until a "significant" wave amplitude (about 10^{-6} of the initial amplitude) has reached the end of this box. The run is stopped, and a new section of grid in y is added on. We continue this process in gradual steps until the time that we start to underresolve the phase mixing in x. (This time is determined by the size of the grid in x as we shall see later.)

As noted previously, we impose perfectly reflecting boundary conditions in x. For our system of equations this requires that u_x, b_x, and $\partial b_z/\partial x$ be zero at $x = 0$ and $x = x_m$. For a symmetric pulse centered at $y = 0$ we require u_y, b_y, $\partial u_x/\partial y$, $\partial b_x/\partial y$, and $\partial b_z/\partial y$ to be zero. Moreover, we need only solve in the half space $y > 0$. We use these same latter conditions at $y = y_m$ (the far end of the waveguide) for convenience, even though, by the previous discussion on our open conditions, they will have little impact.

Since we are interested in the wave propagation properties of the waveguide, we do not seek to model how an initial perturbation enters the box. We therefore start with a perturbation of the form

$$u_x(x, y, t = 0) = \frac{1}{2}\sin(k_x x)[1 + \cos(\pi y/\lambda_{yo})], \tag{16}$$

$0 \le y \le \lambda_{yo}$, $u_x(x, y, t = 0) = 0$ otherwise, and $k_x = 2\pi/\lambda_x$. For the cases we shall examine both λ_x and λ_z

are set to 2. In y this perturbation is a maximum at and symmetric about $y = 0$, falls to zero at $y = \lambda_{yo}$, and is zero everywhere else in y. In x the perturbation is simply one half of a sine cycle. The values of λ_{yo} that we shall detail are 1, 1/4, and 1/8, all normalized by x_m, of course. We consider several width initial conditions to see how robust the resonant coupling to Alfvén waves is.

4. Results

As mentioned previously, a limit on the time we can run the simulation for is provided by the phase mixing length. Phase mixing refers to the process where neighboring field lines drift out of phase as a result of their natural frequency depending on x namely $\omega_A = \pm k_z V(x)$. Defining the phase mixing length in x (L_{ph}, say) as the length over which the phase of neighboring Alfvén waves differ by 2π, we find

$$L_{ph} \approx 2\pi/(td\omega_A/dx), \tag{17}$$

and L_{ph} decreases with time. To have an accurate simulation, we must always resolve the phase mixing length. To follow the results further in time becomes increasingly demanding on computer time since a smaller grid size in x (to resolve L_{ph}) requires an accordingly reduced time step.

In practice, a uniform grid is employed in x, and so the grid size in x is chosen to resolve the smallest $L_{ph}(x)$, which may result in inefficient gross overresolution where $L_{ph}(x)$ is greater than the minimum $L_{ph}(x)$. To avoid such inefficiency, we choose a medium that has a phase mixing length which is independent of x. This is achieved by a density profile producing the following Alfvén speed variation:

$$V(x) = (1 - \frac{x}{x_o}). \tag{18}$$

In general, several Alfvén resonances may be excited. In order to study the coupling process more clearly we chose the medium to have only one resonance. This was achieved by setting $x_o = 1.3$ in our dimensionless units. This results in an Alfvén speed that is 1 at $x = 0$ and falls linearly to 3/13 (0.231) at the outer boundary $x = 1$. For these parameters the $k_y \approx 0$ fast mode should drive a resonance at $x \approx 0.357$, where the natural Alfvén wave ($\omega_A \approx 2.28$) has a time period of approximately 2.76.

Waveguide Dispersion

From the description of fast mode dispersion in section 2 we anticipate that the b_z (fast mode) disturbance which remains at $y = 0$ should be composed of fast waveguide modes with $k_y = 0$. A time history of $b_z(x = 0.75, y = 0, t)$ is shown in Figure 4. A Fourier transform reveals four significant frequencies at $\omega_1 = 2.28$, $\omega_2 = 3.77$, $\omega_3 = 5.18$, and $\omega_4 = 6.91$. These compare favourably with the first four eigenfrequencies obtained from an evaluation of the phase integral (9)

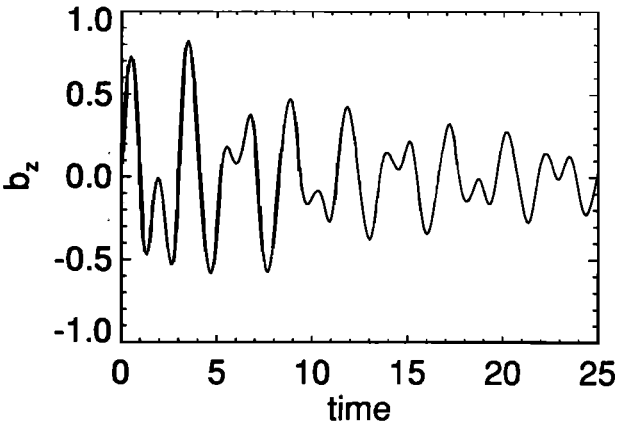

Figure 4. A plot of b_z against time at $x = 0.75$, $y = 0$ for $\lambda_{yo} = 1.0$.

yielding 2.19, 3.77, 5.26, and 6.83, respectively. The first two eigenfrequencies may be read off Figure 2 at $k_y = 0$.

On Figure 3 we have also plotted (in arbitrary units) the magnitude of the Fourier k_y spectrum of the initial disturbance, which is calcualted as $\int_0^\infty u_x(x, y, t = 0)\cos(k_y y)dy$. We see that for $\lambda_{yo} = 1$ only low values of k_y ($\lesssim 6$) are significant. The spatial dispersion of these k_y components can be seen in Figure 5 which shows a slice of b_z in y at $x = 0.75$ and time $t = 25$. The leading edge around $y = 11$ corresponds to a wave number in y of 4.5 obtained by direct measurement from the figure. From the WKB group velocity diagram (Figure 3) we find that this wave number is indeed close to the fastest velocities. For $k_y = 4.5$ we can estimate the frequency and group velocity of the modes from Figures 2 and 3, respectively. The first, second, and third (not shown in the figures) eigenmodes have group velocities and eigenfrequencies of 0.27, 0.33, 0.29 and 3.0, 4.4, 5.91, respectively for $k_y = 4.5$. The second harmonic in x has the greatest group velocity, so we would expect the disturbance in the leading edge at $y \approx 11$ to be predominantly second harmonic.

The above assertion is supported by Figure 6, which shows b_z as a function of time for $x = 0.75$ and $y = 5.625$. We see no signal until approximately $t = 8$.

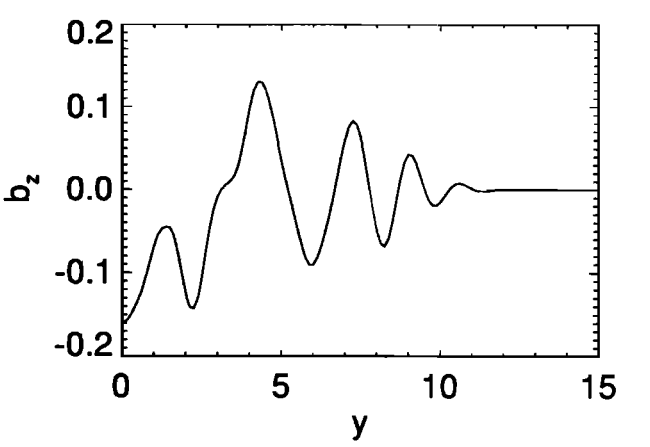

Figure 5. A plot of b_z against y at $x = 0.75$, $t = 25$ for $\lambda_{yo} = 1.0$.

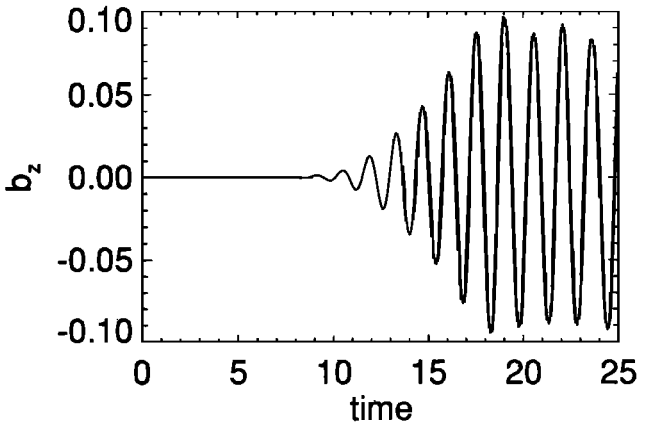

Figure 6. A plot of b_z against time at $x = 0.75$, $y = 5.625$ for $\lambda_{yo} = 1.0$.

Thereafter an oscillatory signal grows and eventually saturates. At early times in the signal a period of about 1.43 is found (from direct measurement off Figure 6), giving a frequency of 4.4, which is an excellent match to the frequency of the second eigenmode given above. Furthermore, cross sections in x (not presented here) in the leading edge have a structure corresponding to the second eigenmode. Figure 6 also reveals a small but significant frequency decrease with time (of about 10 percent), a result of the tendency to be left with the small wave number, lower-frequency components at later times (see *Wright* [1994] for a detailed discussion of spatial and temporal dispersion).

To emphasize the dispersive properties of the waveguide, we now consider the narrowest initial condition $\lambda_{yo} = 0.125$. From Figure 3 we see that this condition contains significant k_y components beyond the maximum group velocity. The dispersive structure of this initial fast mode will be quite different to the $\lambda_{yo} = 1$ condition which only contained significant k_y components below the group velocity maximum. Figure 7a shows $b_z(0.75, y, 25)$. The leading edge ($y \approx 13$) is quasi-sinusoidal since it corresponds to the fastest propagating mode (i.e., a single k_y value). Behind the leading edge (e.g., $7 \lesssim y \lesssim 12$) we see fluctuations corresponding to modes with velocities slightly lower than the maximum. For example, the $n = 2$ modes with $k_y = 3$ and 20 *both* have group speeds of the order of 0.3, thus a combination of large and small scale lengths are observed simultaneously in this interval. For our waveguide the asymptotic group velocity for large k_y is 0.231. Modes traveling at this speed will reach $y \approx 5.9$ by $t = 25$. This position is marked by the vertical dashed line in Figure 7a. This line clearly separates the smallest spatial scales immediately beyond $y = 5.9$ to the longer wavelength features below $y = 5.9$. Below $y = 5.9$ we see only large spatial scales corresponding to the small $k_y (\lesssim 3)$, and the features are thus similar to Figure 5. The WKB estimate for the group velocity dependence of k_y clearly matches this very well. All the small spatial scales travel at least as fast as the asymptotic group velocity, while the long wavelengths go more slowly than this particular speed. This is reinforced by Figure 7b which displays $b_z(0.75, 4.125, t)$. We see high frequencies divided from low frequencies at time $t \doteq 17.334$, the time by which information traveling at the asymptotic group speed would reach $y = 4.125$.

In summary, we see that the features expected from the WKB dispersion and group velocity diagrams agree well with our simulations and are a useful, practical method of discussing fast mode propagation in our waveguide.

The Alfvén Resonance

We now move on to consider the features of the Alfvén resonance itself in more detail. If our problem had only an x dependence ($k_y = 0$), then the fast and Alfvén modes decouple exactly. The linear fast mode energy density E_f, say, and the Alfvén mode energy density E_a, say, are

$$E_f = \frac{1}{2}(\rho {u_x}^2 + {b_x}^2 + {b_z}^2),$$

$$E_a = \frac{1}{2}(\rho {u_y}^2 + {b_y}^2).$$

Although this split is not exact when $k_y \neq 0$, it remains a fairly good diagnostic as to the energy partition in the system.

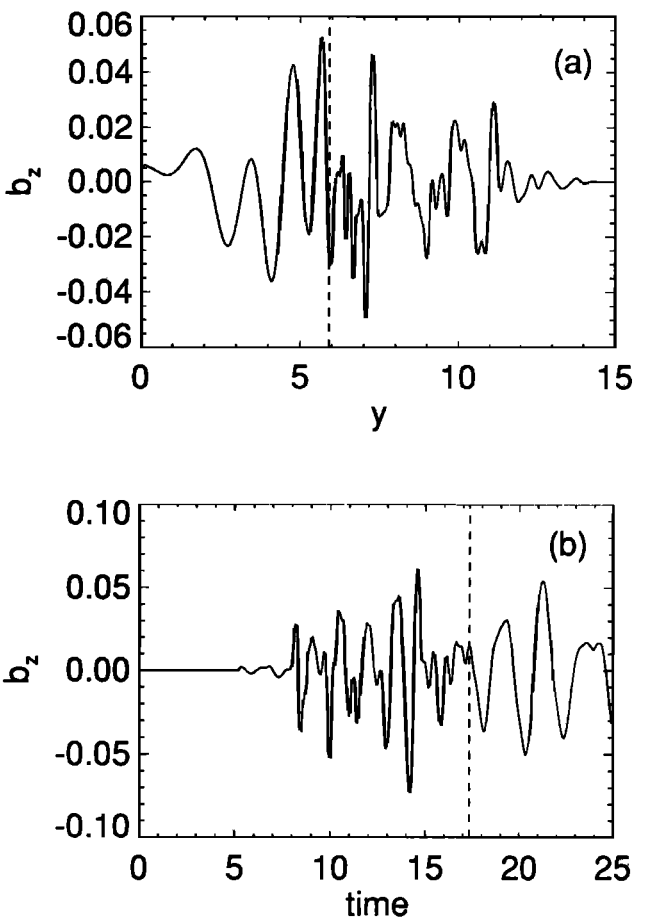

Figure 7. Plots of b_z as a function of (a) y at $x = 0.75$ and $t = 25$, and (b) time at $x = 0.75$ and $y = 4.125$, both for $\lambda_{yo} = 0.125$.

Figure 8 plots the integral of E_f and E_a over the (x, y) plane against time. All the energy of the perturbation initially resides in E_f. As is clear, with increasing time there is a transfer of energy from the fast mode to the Alfvén resonance.

The characteristic development of an Alfvén resonance is shown by the slices of u_y in x at $y = 0.625$ for the three times $t = 5$, 15, and 25 in Figures 9a, 9b, and 9c, respectively. For this case the resonant position for the first eigenmode ($k_y = 0$) is marked by a vertical dashed line at $x = 0.357$ in each figure. The growth of the resonance in the vicinity of this line is quite evident. Estimates of the phase mixing lengths (L_{ph}) from (17) at each time are marked by the horizontal lines. The values are 0.58, 0.173, and 0.104 at increasing times. These clearly match well the observed mixing lengths that we see.

Figures 10a, 10b, and 10c are contours of the total energy density ($E_f + E_a$) at $t = 25$ plotted for the λ_{yo} values of 1.0, 0.25, and 0.125, respectively. Here the horizontal dashed line marks the position of the resonance associated with the $k_y = 0$ first eigenmode, while the vertical dashed line marks λ_{yo}, the furthest extent of the initial perturbation in y. It is apparent that the resonant position is insensitive to the initial conditions. We also note that the resonant peaks tend to lie slightly above the horizontal line. This results because the $k_y = 0$ modes do not propagate beyond λ_{yo}. It is the modes with small but nonzero values of k_y that drive the resonances in the region $y > \lambda_{yo}$. These modes have slightly higher frequencies than $k_y = 0$ modes and hence tend to drive resonant Alfvén modes at slightly lower values of x. We note that it is only the k_y values slightly displaced from $k_y = 0$ that can drive a resonance. Only modes with these wave numbers linger long enough (e.g. for a few cycles) to establish a resonance. The larger k_y modes propagate more or less down the waveguide in x, and hence cannot drive any single field line coherently for a significant time.

In Figure 10a for the broadest initial condition the resonance within λ_{yo} is the dominant feature. There is also a much weaker secondary resonance centered at

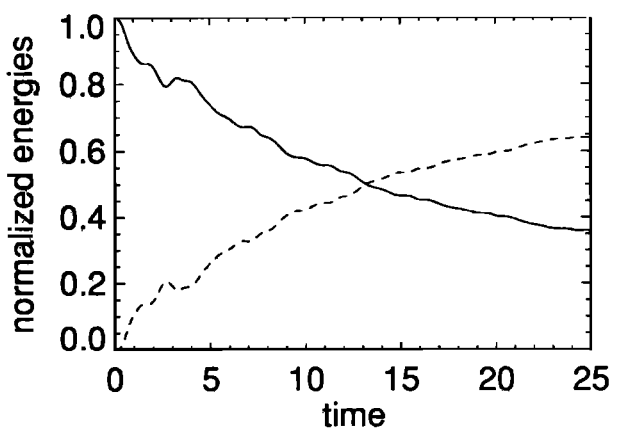

Figure 8. Normalized time histories of the energies E_f (solid curve) and E_a (dashed curve) integrated over the (x, y)-plane (see text) for $\lambda_{yo} = 1$.

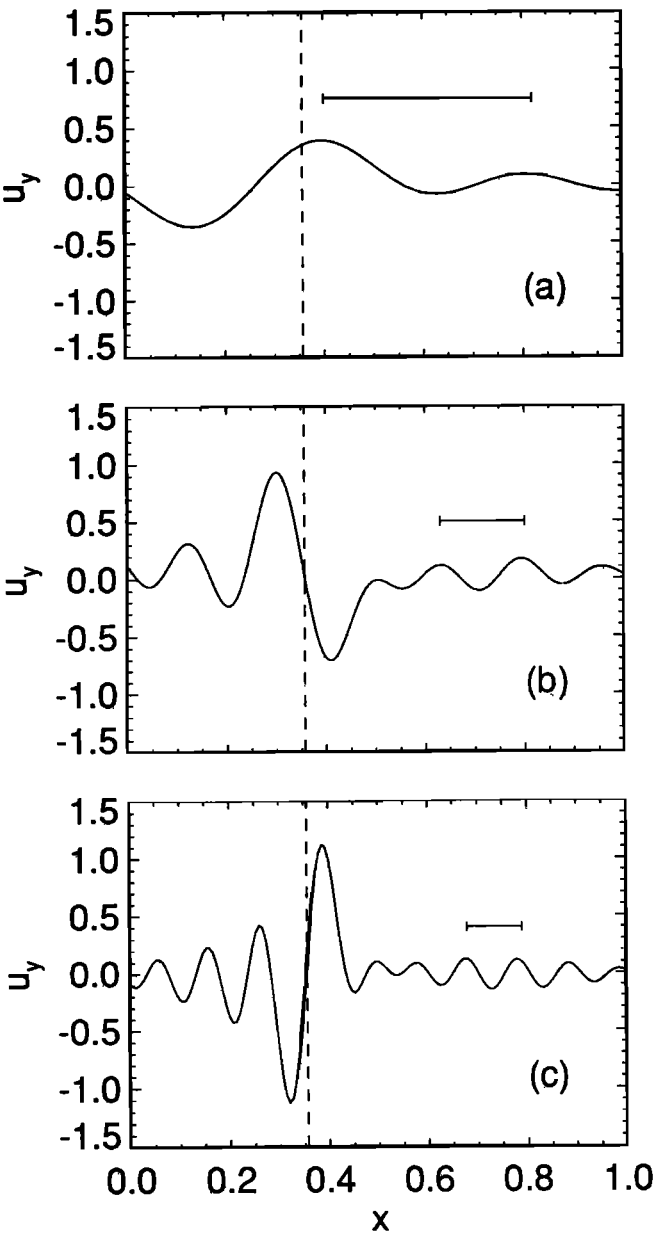

Figure 9. Profiles in x of u_y at $y = 0.625$ for the times (a) 5, (b) 15, and (c) 25 for $\lambda_{yo} = 1.0$. The vertical dashed line locates the position of the resonance (based upon the $k_y = 0$ fundamental fast mode), while the horizontal line indicates the characteristic phase mixing length at that time.

$y \approx 2.5$. The other weak features ($0.5 \lesssim x \lesssim 1.0$) are the remnants of the fast mode energy. In Figure 10b there is still a strong resonant peak within λ_{yo}. However we now see two extra resonant peaks *outside* this region at $y \approx 0.75$ and 2.5, with the furthest arising nearly ten times λ_{yo} down the waveguide.

In the limit $\lambda_{yo} \to \infty$ ($k_y \to 0$) the initial disturbance (16) is entirely associated with the fast mode. In the opposite limit $\lambda_{yo} \to 0$ ($k_y \to \infty$) the initial condition is purely Alfvénic, representing the decoupled poloidal mode [*Dungey*, 1967]. For intermediate values of λ_{yo} our initial disturbance may be thought of as a combination of fast and Alfvén waves. In Figure 10a

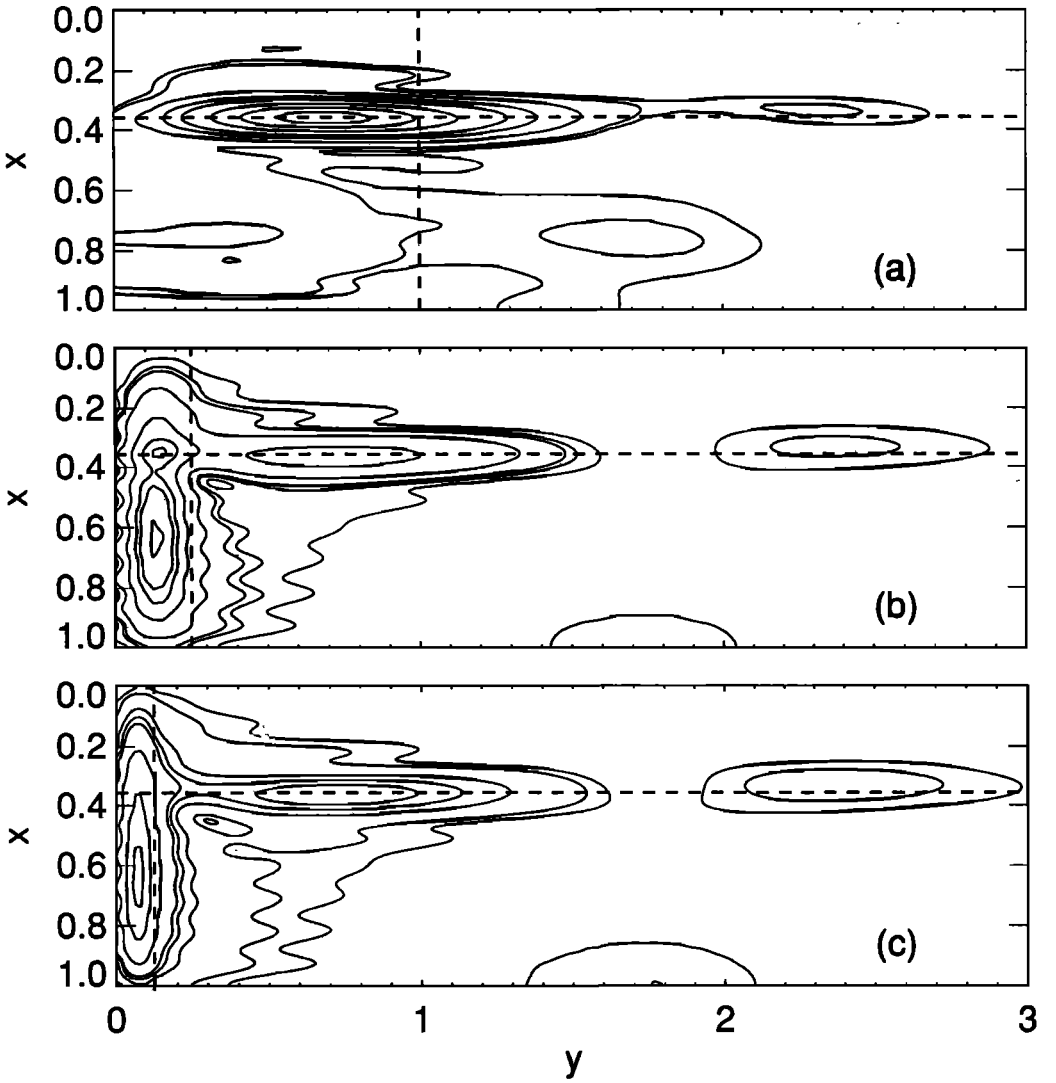

Figure 10. Contours of the total energy density ($E_f + E_a$) at $t = 25$ for (a) $\lambda_{yo} = 1.0$, (b) $\lambda_{yo} = 0.25$, and (c) $\lambda_{yo} = 0.125$. The horizontal dashed line locates the expected resonance positions, while the vertical dashed line indicates λ_{yo} for each case.

($\lambda_{yo} = 1$) the initial condition is predominantly fast in character, whereas in 10b ($\lambda_{yo} = 0.25$) there is a significant Alfvénic component. This manifests itself in Figure 10b as the second peak within the initial disturbance ($y < 0.25$) near $x \approx 0.6$. This peak represents Alfvén energy left over from the original perturbation and is not resonantly excited. This feature is even more dramatic in Figure 10c for $\lambda_{yo} = 0.125$. The resonance within λ_{yo} is now subsidiary to the excess Alfvén energy. We also see that the secondary resonances appear at similar positions down the waveguide, suggesting that they may also be insensitive to the initial conditions.

In Figure 11 we emphasize the resonances by plotting slices of E_a along a line through the resonances just on the $x = 0$ side of the $k_y = 0$ resonant location ($x \approx 0.334$) for the three cases in Figure 10. The vertical line again marks λ_{yo}. The resonance within the initial disturbance ($y < \lambda_{yo}$) is still the major feature. However, especially for the higher wave number perturbations, the presence of the secondary resonances is quite clear.

5. Conclusions

We have not attempted to employ realistic magnetospheric parameters in this preliminary study of MHD waves in a nonuniform waveguide. Rather, we have attempted to establish the basic processes that operate in such systems, namely dispersion and mode coupling. The theoretical basis for our understanding is the waveguide dispersion obtained from a WKB approximation. The WKB diagrams such as those in Figures 2 and 3 provide a reliable basis that may be employed to explain the behavior of the fast and Alfvén modes.

The numerical dispersive signatures of the fast mode in both space and time agree well with the expectations

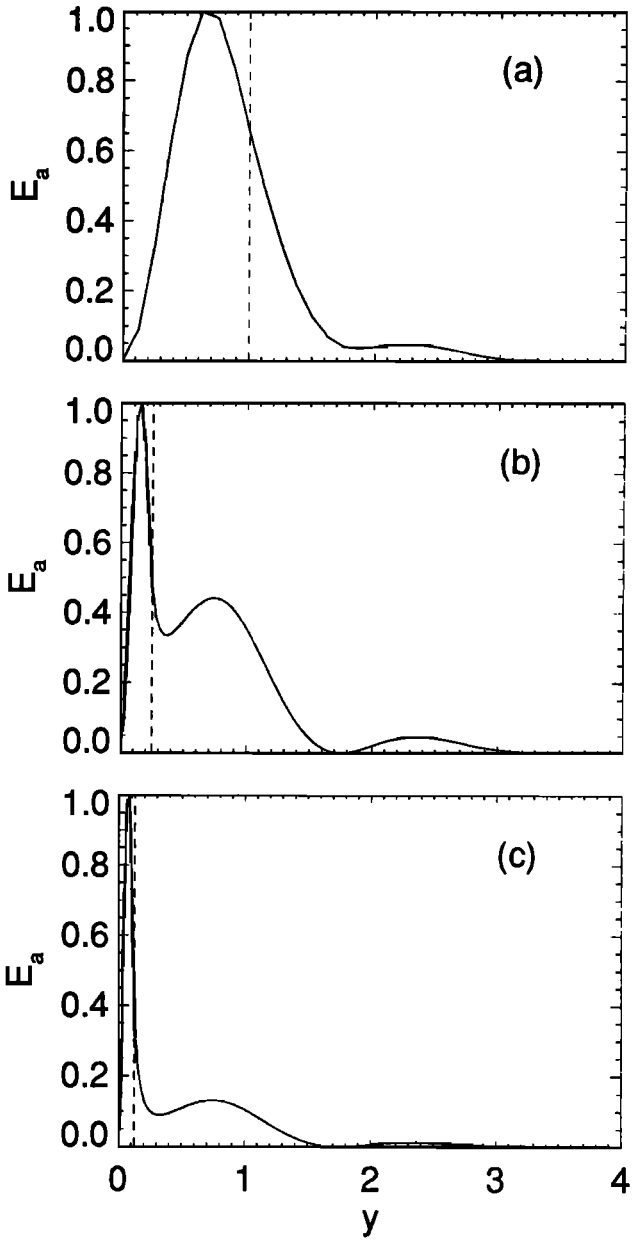

Figure 11. Profiles of E_a against y along $x = 0.334$ for the instances in Figures 10a-10c , respectively. The vertical dashed line again marks the position of λ_{yo}. The energy densities have been separately normalised in each case for convenience.

of the WKB theory. Indeed, identifying signatures like those in Figure 7b in data could provide useful information about the magnetosphere, such as the asymptotic group velocity (equal to $V(x_m)$). Whether or not transitions like the one indicated by the dashed line in Figure 7b are observed in data, constrains the initial extent of the fast mode in y, and may shed some light on the origin of the fast mode.

Probably the principal result established in this paper is that an Alfvén resonance associated with the $k_y = 0$ fast waveguide modes evolves independent of the initial conditions, as proposed by *Wright* [1994]. This agrees with observations where the resonances ("pulsations") are robust to a whole range of conditions.

Although the approximate WKB theory has enabled us to make sense of some of our results, it is by no means complete. There is clearly a measure of complexity in even the modest nonuniformity considered here, in particular the development of secondary resonances at apparently discrete locations further down the waveguide. Furthermore, our Alfvén spectrum has been deliberately chosen so as to allow the possibility of only a single resonance within the waveguide. The hidden complications in a more "realistic" configuration will be reported in a future publication.

From a computational standpoint it transpires that the modeling of an open system in the way we have done is very intensive for both processing time and eventual data storage. As we intimated earlier there are three limiting factors. The first is the ultimate length of the waveguide to allow the open-endedness to be dealt with satisfactorily, since we do not feel that the absorption of outgoing MHD waves by present methods are sufficiently simple to implement or particularly efficient. Significant computer time could be saved if a suitable absorbing boundary condition at the end of the waveguide could be devised. The second limitation is the phase mixing lengths which, as we have seen, reduce inversely with time. (This problem can be avoided by the inclusion of dissipation in the magnetospheric medium [*Inhester*, 1987], although ionospheric resistivity is probably the most important sink of energy.) The third, and perhaps the most severe, is the resolution of the fast mode eigenfunctions in x for a nonuniform waveguide. The latter limitation worsens as the extent in y of the initial disturbance λ_{yo} is reduced, resulting in underresolution of the eigenfunctions. In the simulations this is seen as small but finite oscillations on the scale size of the mesh. The cure is simply more points in x (as we have verified), but the price is significantly increased processing time and data storage.

On a final positive note we would say that despite the possible pitfalls the simulations are relatively simple to perform, and furthermore the WKB theory provides a solid foundation on which to interpret any modeling. All our efforts have been performed on workstations.

Acknowledgments. This work was carried out while one of us (A.N.W.) was supported by a UK SERC Advanced Fellowship.

The Editor thanks B.G.R. Harrold and another referee for their assistance in evaluating this paper.

References

Allan, W., S. P. White, and E. M. Poulter, Impulse-excited hydromagnetic cavity and field-line resonances in the magnetosphere, *Planet. Space Sci., 34,* 371, 1986.

Chen, L., and A. Hasegawa, A theory of long-period magnetic pulsations, 1, Steady state excitation of field line resonance *J. Geophys. Res., 79,* 1024, 1974.

Dungey, J. W., Hydromagnetic waves, in *Physics of Geomagnetic Phenomena,* vol. 2, edited by S. Mat-

sushita and W. H. Campbell, p. 913, Academic, San Diego, Calif., 1967.

Edwin, P. M., B. Roberts, and W. J. Hughes, Dispersive ducting of MHD waves in the plasma sheet: A source of Pi2 wave bursts, *Geophys. Res. Lett., 13,* 373, 1986.

Harrold, B. G., and J. C. Samson, Standing ULF modes of the magnetosphere: A theory, *Geophys. Res. Lett., 19,* 1811, 1992.

Hopcraft, K. I., and P. R. Smith, Magnetohydrodynamic waves in a neutral sheet, *Planet. Space Sci., 34,* 1253, 1986.

Inhester, B., Numerical modeling of hydromagnetic wave coupling in the magnetosphere, *J. Geophys. Res., 92,* 4751, 1987.

Kivelson, M. G., and D. J. Southwood, Resonant ULF waves: A new interpretation, *Geophys. Res. Lett., 12,* 49, 1985.

Kivelson, M. G., and D. J. Southwood, Coupling of global magnetospheric MHD eigenmodes to field line resonances, *J. Geophys. Res., 91,* 4345, 1986.

Lee, D. H., and R. L. Lysak, Magnetospheric ULF wave coupling in the dipole model: The impulsive excitation, *J. Geophys. Res., 94,* 17,097, 1989.

McClay, J. F., and H. R. Radoski, Hydromagnetic propagation in a theta-model geomagnetic tail, *J. Geophys. Res., 72,* 4525, 1967.

Roberts, B, P. M. Edwin, and A. O. Benz, On coronal oscillations, *Astrophys. J., 279,* 857, 1984.

Samson, J. C., B. G. Harrold, J. M. Ruohoniemi, and A. D. M. Walker, Field line resonances associated with MHD waveguides in the magnetosphere, *Geophys. Res. Lett., 19,* 441, 1992.

Southwood, D. J., Some features of field line resonances in the magnetosphere, *Planet. Space Sci., 22,* 483, 1974.

Walker, A. D. M., J. M. Ruohoniemi, K. B. Baker, and R. A. Greenwald, Spatial and temporal behaviour of ULF pulsations observed by the Goose Bay HF radar, *J. Geophys. Res., 97,* 12,187, 1992.

Wright, A. N., Dispersion and Wave Coupling in Inhomogeneous MHD Waveguides, *J. Geophys. Res., 99,* 159, 1994.

Zalesak, S. T., Fully multidimensional flux-corrected transport algorithms for fluids, *J. Comput. Phys., 31,* 335, 1979.

G. J. Rickard and A. N. Wright, Department of Mathematical and Computational Sciences, University of St. Andrews, St. Andrews, Fife KY16 9SS, Scotland, U.K. (e-mail:grahamr@dcs.st-andrews.ac.uk; andy@dcs.st-andrews.ac.uk)

(Received November 29, 1993; revised February 3, 1994; accepted March 8, 1994.)